Hydrogen-Bonding Dynamics between Adjacent Blades in G-Protein β-Subunit Regulates GIRK Channel Activation

Tooraj Mirshahi, Diomedes E. Logothetis, and Avia Rosenhouse-Dantsker
Department of Physiology and Biophysics, Mount Sinai School of Medicine, New York, New York 10029

ABSTRACT Functionally critical domains in the $\beta\gamma$-subunits of the G-protein ($G\beta\gamma$) do not undergo large structural rearrangements upon binding to other proteins. Here we show that a region containing Ser^{67} and Asp^{323} of $G\beta\gamma$ is a critical determinant of G-protein-gated inwardly rectifying K^+ (GIRK) channel activation and undergoes only small structural changes upon mutation of these residues. Using an interactive experimental and computational approach, we show that mutants that form a hydrogen-bond between positions 67 and 323 do not activate a GIRK channel. We also show that in the absence of hydrogen-bonding between these positions, other factors, such as the displacement of the crucial $G\gamma$ residues Pro^{60} and Phe^{61}, can impair $G\beta\gamma$-mediated GIRK channel activation. Our results imply that the dynamic nature of the hydrogen-bonding pattern in the wild-type serves an important functional role that regulates GIRK channel activation by $G\beta\gamma$ and that subtle changes in the flexibility of critical domains could have substantial functional consequences. Our results further strengthen the notion that the dynamic regulation of multiple interactions between $G\beta\gamma$ and effectors provides for a complex regulatory process in cellular functions.

INTRODUCTION

G-protein-coupled receptor activation leads to dissociation of $G\alpha$ from the $G\beta\gamma$-subunits, which in turn interact with specific effectors. G-protein interaction with effectors leads to downstream signal transduction pathways that are essential to cellular function. Therefore, understanding the detailed mechanism of such interactions is critical. Many signaling molecules undergo significant structural rearrangements during their activation process. These include those that shed their regulatory subunits to expose catalytic subunits. Many proteins are phosphorylated on specific residues to assume the correct information to interact with downstream effectors. Recent data have shown that contrary to the conventional view $G\alpha$ and $G\beta\gamma$ may not completely dissociate upon activation and remain in contact during signaling (1). Although this partial dissociation exposes surfaces on both $G\alpha$ and $G\beta\gamma$ that have been implicated in interaction with effectors (2,3), there are several examples of functionally critical domains on $G\beta\gamma$ as well as $G\alpha$ that are exposed in the heterotrimer (4–6). Interestingly, $G\beta\gamma$ does not undergo major structural rearrangements upon activation (7–10). It is therefore likely that subtle changes in these domains are responsible for differences in protein function.

The G-protein-gated inwardly rectifying K^+ (GIRK or Kir3) channels were the first of several effectors that were found to be regulated directly by the $G\beta\gamma$-subunits (11–13). GIRK channels are homomers or heteromers of four different subunits (GIRK1-4) that have been identified so far (14–18). Heteromers of GIRK1 and GIRK4 channels constitute K_{ACh} (19) that controls atrial cell excitability and heart rate through activation of muscarinic receptors by the vagus nerve. Similar to other effectors of $G\beta\gamma$, several interaction sites between GIRK channels and $G\beta\gamma$ have been identified. Some of these sites are exposed on the surface of the heterotrimeric G-protein, whereas others are exposed on the $G\beta$ surface only upon dissociation from the $G\alpha$-subunits (2,4,20,21). However, it is not known how any of these interactions control channel function.

The presence of a high-resolution crystal structure of $G\beta\gamma$ (7) aids in interpretation of structure-function data. Cocrystals between $G\beta\gamma$ and $G\alpha i1$ (8), the retinal $G\beta\gamma$ effector, phosducin (9), and the PH domain of the β-Adrenergic Receptor Kinase 1 (βARK1-PH) (10) have also been resolved. Detailed study of the cocrystals shows that there are multiple interaction sites between $G\beta\gamma$ and $G\alpha i1$, phosducin, and βARK1-PH. The crystal structures of $G\beta\gamma$ in either free form or those bound to $G\alpha i1$, phosducin, or βARK1-PH are very similar. These structures support the notion that the $G\beta\gamma$ dimer has a rather rigid structure and does not undergo major structural rearrangements upon interaction with effectors. Rather, $G\beta\gamma$ is likely to undergo only subtle structural changes, and clues to these changes could be found in its dynamic characteristics. However, static representations of structures, such as in the x-ray crystal, lack dynamic information. $G\beta\gamma$ is solvated and like other solvated molecules it fluctuates among different conformations. Upon crystallization, however, the protein adopts a single specific structure. To provide further refinement and information on the dynamic nature of protein structures, computer simulations can be utilized. Here we use molecular dynamics (MD) simulations and site-directed mutagenesis and examine detailed structural elements in $G\beta\gamma$ that are critical in activation of GIRK channels.

Submitted June 22, 2005, and accepted for publication December 1, 2005.

Tooraj Mirshahi and Avia Rosenhouse-Dantsker contributed equally to this work.

Address reprint requests to Avia Rosenhouse-Dantsker, E-mail: avia.rosenhouse-dantsker@mssm.edu.

0006-3495/06/04/2776/10 $2.00

doi: 10.1529/biophysj.105.069302

MATERIALS AND METHODS

Simulations

The primary hydration shell (PHS) method (22) provides both an efficient representation of solvation effects and a flexible nonspherical restraining potential. To replace the bulk representation of the solvent, a restraining force that balances the instantaneous pressure inside the primary solvent shell is applied. The MD simulations were performed using CHARMM, version 26 (23). The initial structure of the G-protein was based on the crystallographic structure, PDB code 1GP2 (8). The region we examined was composed of the two loops that include position 67 (residues 63–70) and 323 (residues 320–327) and residues in an adjacent loop (residues 82–88) and residues in their vicinity that belong to the γ-subunit of the G-proteins (residues 47–50; 59–61). This region was surrounded by a 30-Å sphere of water molecules whose origin was located at its center of mass. Water molecules located within 2.6 Å or further than 15 Å from these residues were deleted, and the combined system was subjected to energy minimization. After removing all waters located 5.5 Å from the examined region and the γ-subunit residues in their vicinity, the system was further minimized. The remaining G-protein was surrounded by a 5 Å shell, which was minimized and then fixed during the simulation along with all other residues of the G-protein that were not included in the examined region. This prevented the water shell from escaping from the region examined to the highly hydrophilic residues of the G-protein. After heating the system to 300 K, the structure was equilibrated and an MD simulation was carried out for 1.2 ns, with a restraining force of 0.95 Kcal/mol Å.

Hydrogen-bonding

The cutoffs for hydrogen-bonding used are as follows: the hydrogen-acceptor distance is ≤2.5 Å, and the donor-hydrogen-acceptor angle is above 90° (24). The total percentage of hydrogen-bonding in Tables 1, 3, and 4 is the percentage of structures that form any hydrogen-bond (one or more) between positions 67 and 323 (or 325 in the S67Y mutant).

cDNAs and mutants

All of the cDNAs used were subcloned into pGEMHE to accommodate sufficient expression in oocytes. Mutations were made using the QuikChange method (Stratagene, La Jolla, CA) using high fidelity *Pfu* polymerase for 12–16 cycles only. All mutations were confirmed by DNA sequencing (Cornell University Sequencing Facilities, Ithaca, NY).

TABLE 1 Hydrogen-bonding data between position 67 and position 323 based on the different Gβγ crystal structures

PDB code	HN(Asp^{323}) –OG(Ser^{67}) distance (Å)	OD1(Asp^{323}) –HG1(Ser^{67}) distance (Å)	OD2(Asp^{323}) –HG1(Ser^{67}) distance (Å)	Minimal distance (Å)	Total % of H-bonding
1A0R	2.1	2.3	2.9	2.1	
1B9X	2.2	2.4	2.1	2.1	
1B9Y	2.3	2.0	2.6	2.0	
1GG2	2.2	2.2	2.9	2.2	
1GOT	2.2	2.5	2.8	2.2	
1GP2	2.2	2.1	2.7	2.1	
1OMW	2.1	1.9	3.0	1.9	
1TBG_A	2.2	2.6	2.8	2.2	
1TBG_B	2.0	2.6	2.7	2.0	
1TBG_C	2.0	2.3	2.9	2.0	
1TBG_D	2.1	2.3	3.1	2.1	
2TRC	2.1	2.0	2.6	2.0	
Average	2.1 ± 0.1	2.3 ± 0.2	2.8 ± 0.3	2.1 ± 0.1	100.0%

Expression in oocytes

cDNA constructs were linearized and subjected to in vitro transcription using the mMessage mMachine kit (Ambion, Austin, TX). The resulting cRNAs were quantified by comparison of two dilutions to a standard on a formaldehyde gel. Oocytes were isolated from *Xenopus laevis* frogs, enzymatically digested with collagenase, and incubated in ND-96 solution containing calcium and nutrients (25). Oocytes were injected with cRNAs, 2 ng each of GIRK1/GIRK4, and 2 ng of each G-protein subunit or mutant. After injection, oocytes were kept for 48–96 h in an 18°C incubator before recordings.

Electrophysiology

Two-electrode voltage clamp recordings were carried out as previously described (26). Briefly, the oocytes were placed in a chamber and perfused with a solution containing high potassium (96 mM). Currents were recorded using a voltage step protocol alternating between −80 and +80 mV (control current). Barium (3 mM) was used to measure the leftover current that was not inwardly rectifying (barium-insensitive current). We determined the inwardly rectifying current by subtracting barium-insensitive current from the control current at −80 mV.

Immunoblot analysis

The N-termini of wild-type (WT) and mutant Gβ-subunits were tagged with a Flag epitope (fGβ1). After two-electrode voltage clamp recordings, oocyte membranes were isolated as previously described (27). Expression levels for each Flag-tagged Gβ protein were detected by immunoblotting using a mouse anti-Flag antibody. Three different batches of oocytes were tested for expression levels.

Immunoprecipitation and trypsin protection assay

For trypsin assays, oocytes were injected with Flag-tagged Gβ1, fGβ1, with or without Gγ2 as well as Flag-tagged mutant Gβ1. Membranes were collected as described (27). fGβ1 was immunoprecipitated overnight at 4°C in lysis buffer containing 1% NP40 using the Flag (M2) Agarose Affinity Gel (Sigma, St. Louis, MO). The immune complex was washed 3× using lysis buffer. A fraction of the beads was subjected to partial digestion by 30 μg/ml trypsin for 30 min at 37°C. The reaction was terminated by addition of loading buffer. Samples were boiled, centrifuged, and subjected to SDS-PAGE. Gβ signals were detected using the T-20 antibody to the C-terminus of Gβ (Santa Cruz Biotechnology, Santa Cruz, CA). The bound antibody was detected by horseradish-peroxidase-conjugated goat anti-rabbit IgG, and enhanced chemiluminescence was used to visualize the bands (Pierce, Rockfrod, IL).

RESULTS

The effect of mutagenesis of Ser^{67} and Asp^{323} of Gβ1 on GIRK channel activation

We have previously identified Ser^{67} on Gβ to be critical in the activation of GIRK channels (4). This residue is surface exposed and does not interact with either Gα or Gγ (7,8). Ser^{67} resides in a loop between strands A and B in the second blade of the seven-propeller structure (see Fig. 1, *A* and *B*). It is conserved among all mammalian Gβ-subunits except for Gβ5, where a lysine resides in the homologous position (28). The mutation of Gβ1(S67K) abolished GIRK channel ac-

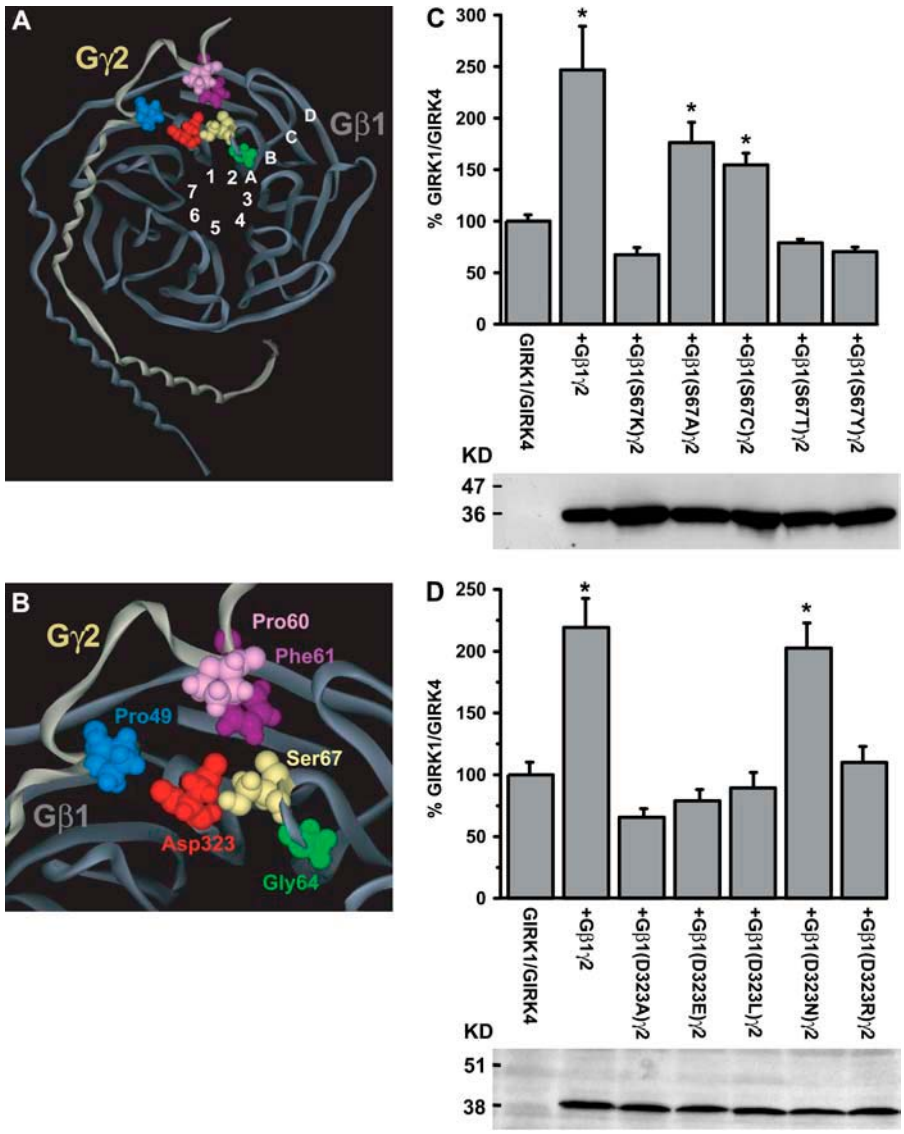

FIGURE 1 (*A*) The atomic coordinates of Gβ1γ2 as determined by x-ray crystallography (8). The seven blades of the Gβ1 propeller are labeled 1–7, and the strands of each blade are labeled A–D. A is the innermost one, whereas D is the outermost strand. Ser^{67} and Gly^{64} on blade 2 of Gβ1 are colored yellow and green, respectively. Asp^{323} on blade 1 is colored red. Pro^{49}, Pro^{60}, and Phe^{61} of Gγ2 are colored blue, magenta, and purple, respectively. (*B*) A close-up of Ser^{67} and its neighboring residues. The segments shown include blades 1 and 2 of Gβ1 (*in gray*) as well as parts of blade 7 and parts of Gγ2 (in *yellow*). The color scheme is as described in *A*. (*C*) Summary data from oocytes expressing GIRK1/GIRK4 in the presence of Gγ2 and WT Gβ1 or mutants of Ser^{67}. Data are expressed as percentage of the control currents at −80 mV in the GIRK1/GIRK4 groups. Expression of WT Gβ1 and mutants S67A and S67C enhanced currents significantly in comparison to GIRK1/GIRK4 alone (* $p < 0.05$, unpaired *t*-test, $n = 9$–17). None of the other mutants significantly enhanced GIRK1/GIRK4 basal current. Western blot detection of an associated Flag-tag confirmed similar expression levels for the WT Gβ1 and its mutants. (*D*) Summary data from oocytes expressing GIRK1/GIRK4 in the presence of Gγ2 and WT Gβ1 or mutants of Asp^{323}. Data are expressed as percentage of the control currents at −80 mV in the GIRK1/GIRK4 groups. Expression of WT Gβ1 and the mutant D323N enhanced currents significantly in comparison to GIRK1/GIRK4 alone (* $p < 0.05$, Unpaired *t*-test, $n = 18$). None of the other mutants significantly enhanced GIRK1/GIRK4 basal current. Western blot detection of an associated Flag-tag confirmed similar expression levels for the WT Gβ1 and its mutants.

tivation by Gβ but did not impair binding (21). A closer analysis of Ser^{67} in the G$\beta\gamma$ structure shows that it interacts with at least two neighboring residues, Gly^{64} and Asp^{323} (Fig. 1, *A* and *B*). We have shown that mutation of Gly^{64} did not affect G$\beta\gamma$ activation of GIRK channels (4). All crystallographic structures of Gβ1 show the presence of hydrogen-bonds between Ser^{67} and Asp^{323}. Asp^{323} is located on blade 1 in the loop between strands A and B and contacts Pro^{49} in Gγ2 (see Fig. 1, *A* and *B*). Pro^{49} in Gγ2 is critical in activation of GIRK channel by Gβ1γ2 (27). We mutated each of the interacting pair of amino acids, Ser^{67} and Asp^{323}, to several different residues to assess the role of this region in GIRK channel activation. Some Gβ mutants, such as S67A, S67C, and D323N, could enhance G$\beta\gamma$-mediated GIRK channel activity, whereas others (S67T, S67Y, D323A, D323E, D323L, and D323R) were ineffective (Fig. 1, *C* and *D*). Immunoblots showed that all these Gβ mutants are expressed properly, and lack of expression cannot account for the inability of the mutants that failed to stimulate GIRK activity. Furthermore Gγ2 protected each mutant in a partial trypsin protection assay (27,29), indicating proper G$\beta\gamma$ dimer formation (data not shown). These findings suggest that the region encompassing Ser^{67} and Asp^{323} is critical in G$\beta\gamma$ function.

Computational analysis of the hydrogen-bonding pattern between Ser^{67} and Asp^{323} of Gβ1

Based on the crystal structures that include Gβ1 (PDB codes 1A0R, 1B9X, 1B9Y, 1GG2, 1GOT, 1GP2, 1OMW, 1TBG, and 2TRC), three possible hydrogen-bonds could be formed between Ser^{67} and Asp^{323} (see Table 1). In accordance with the Gβ1 crystal structures, OG(Ser^{67}) and HN(Asp^{323}) (see Fig. 2 *B*) were within range for hydrogen-bond formation (2.1 ± 0.1 Å). In addition, hydrogen-bonds could be formed between HG1(Ser^{67}) and either OD1(Asp^{323}) (2.3 ± 0.2 Å)

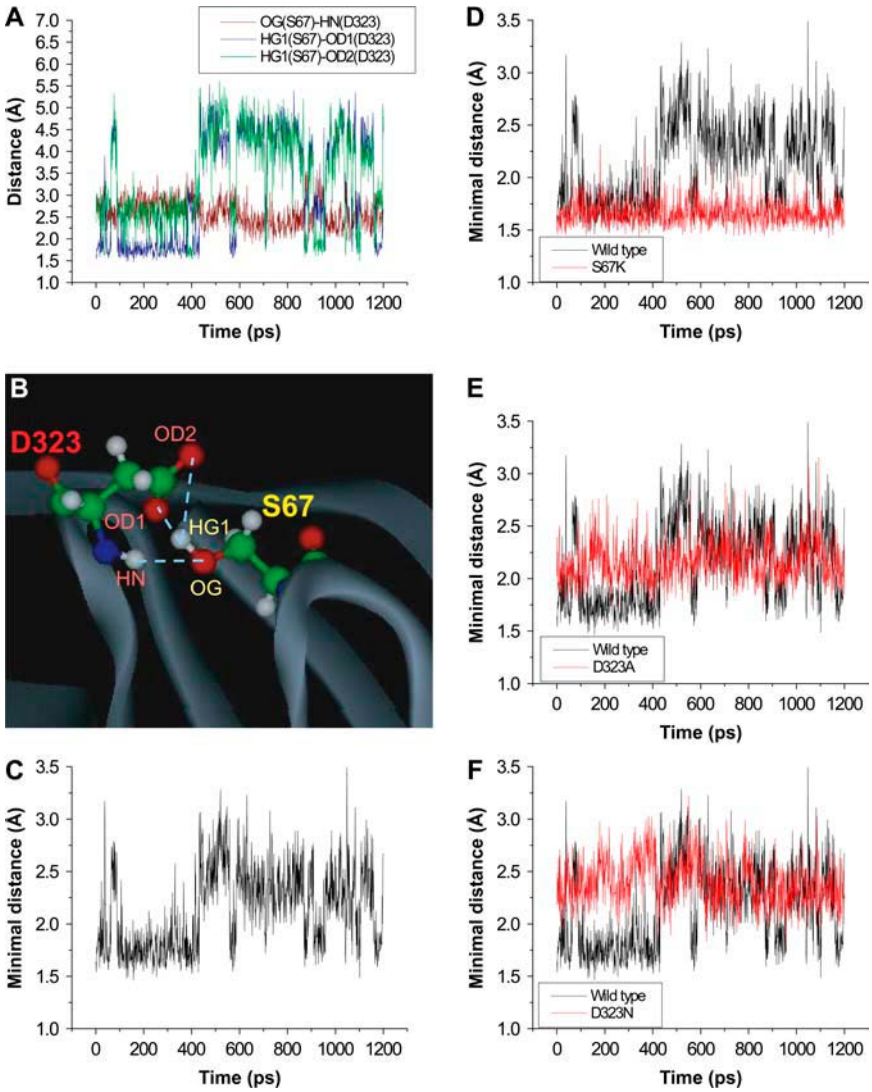

FIGURE 2 (*A*) Hydrogen-bonding distances between Ser^{67} and Asp^{323} as a function of time for the WT G$\beta1\gamma2$. The WT G$\beta1\gamma2$ exhibits three different hydrogen-bonds: HN(Ser^{67})-OG(Asp^{323}), HG1(Ser^{67})-OD1(Asp^{323}), and HG1(Ser^{67})-OD2 (Asp^{323}). (*B*) Ser^{67} and its possible hydrogen-bonds with Asp^{323}: a schematic picture based on the crystallographic structure of G$\beta1\gamma2$ (8). The color scheme is as described in Fig. 1 *A*. (*C*) Minimal distance between Ser^{67} and Asp^{323} as a function of time for the WT G$\beta1\gamma2$. The WT fluctuates between hydrogen-bonded conformations and a nonhydrogen-bonded conformation. (*D*) Minimal distance for G$\beta1$(S67K)$\gamma2$ compared to the WT G$\beta1\gamma2$ as a function of time. Hydrogen-bonds are formed between HZ1, HZ2, and HZ3 of Lys^{67} and OD1 and OD2 of Asp^{323}. In contrast to the WT, the S67K mutant exhibits very small fluctuations around an average minimal distance of 1.7 Å. (*E*) Minimal distance for G$\beta1$(D323A)$\gamma2$ compared to the WT G$\beta1\gamma2$ as a function of time. The D323A mutation exhibits a stable minimal distance with an average of 2.2 Å for a hydrogen-bond between HN of Ala^{323} and OG of Ser^{67}. (*F*) Minimal distance for G$\beta1$(D323N)$\gamma2$ compared to the WT G$\beta1\gamma2$ as a function of time. The D323N mutation exhibits an average minimal distance of 2.4 Å with hydrogen-bonds between HN of Asn^{323} and OG of Ser^{67} and HN of Asp^{322} and OG of Ser^{67}. The D323N exhibits significant periods of time in which there is no hydrogen-bond between position 67 and position 323 (and its neighboring position).

or OD2(Asp^{323}) (2.8 ± 0.3 Å) (Fig. 2 *B*). To evaluate the importance of the distance between positions 67 and 323 and to examine the factors that could explain the functional characteristics of the mutants, we simulated the structure of the WT and mutant proteins using MD. Positions 323 and 67 are located in loops of blades 1 and 2 of G$\beta1$, respectively, and therefore a reliable representation of their environment was required since the solvent plays an integral part in the structure and dynamics of loops. To this end we used the primary hydration shell (PHS) model to provide a minimal but adequate representation of the protein in its natural environment (22). Using this method, we sampled the dynamic characteristics of the WT G$\beta\gamma$ as well as the mutants in 1.2 ns simulations at room temperature. This enabled us to monitor and analyze changes in the hydrogen-bonding pattern between the two loops in blades 1 and 2 upon mutation of either Asp^{323} or Ser^{67} and compare them to the WT G$\beta\gamma$.

Simulation of the WT protein showed that the distance between OG(Ser^{67}) and HN(Asp^{323}) ranged between 1.9 Å and 3.7 Å with an average of 2.6 Å (Fig. 2, *A* and *B*, Table 3). The root mean square (RMS) of the fluctuations was 0.3 Å. The range of distances (2.0–2.3 Å) displayed in the crystallographic structures (Table 1) was contained within a small subpopulation of structures (~15%) that exhibited the shortest distance obtained in the simulation. The large fluctuations in the hydrogen-bond between OG(Ser^{67}) and HN (Asp^{323}) implied that this hydrogen-bond was constantly disrupted: only in 36.4% of the structures obtained in the simulation were these atoms hydrogen-bonded. The two hydrogen-bonds between HG1(Ser^{67}) and OD1(Asp^{323}) and OD2(Asp^{323}) that exist in the crystallographic structures were also observed in the simulation (Fig. 2, *A* and *B*). In the crystallographic structures, the distance between HG1(Ser^{67}) and OD1(Asp^{323}) was 2.3 ± 0.2 Å and varied between 2.0 Å and 2.6 Å, and the distance between HG1(Ser^{67}) and

OD2(Asp^{323}) was 2.8 ± 0.3 Å and varied between 2.1 Å and 3.1 Å. Overall, the distance between HG1(Ser^{67}) and OD1(Asp^{323}) was within hydrogen-bonding range in 67% of the crystal structures, and the distance between HG1(Ser^{67}) and OD2(Asp^{323}) was within hydrogen-bonding range in 8% of the crystal structures. The variation in these distances was larger in the simulated structures than in the crystallographic ones. The average distance HG1(Ser^{67})-OD1(Asp^{323}) obtained in the simulation was 3.2 Å with RMS of fluctuations of 1.2 Å, and the average distance HG1(Ser^{67})-OD2(Asp^{323}) was 3.4 Å with RMS of fluctuations of 1.0 Å. Both these distances fluctuated in the simulation from 1.5 Å to above 5.5 Å and exhibited continuous periods in which these atoms were within hydrogen-bonding distances. OD1(Asp^{323}) was H-bonded to HG1(Ser^{67}) in 38.3% of the structures, and OD2(Asp^{323}) was hydrogen-bonded to HG1(Ser^{67}) in 21.8%. Taking these three different interactions into account, Fig. 2 *C* depicts the minimal distance between Ser^{67} and Asp^{323} for each structure obtained in the simulation. Fig. 2 *C* shows that there were uninterrupted periods in which there was hydrogen-bonding between these residues; but there were also continuous periods in which the minimal distance between Ser^{67} and Asp^{323} exceeded 2.5 Å. The average minimal distance in the simulation was 2.1 Å, which is in agreement with the average minimal distance of the crystal structures. However, the simulation suggests that the hydrogen-bonding pattern is dynamic and displays larger fluctuations than in the crystallographic structures. The RMS of fluctuations in the simulation was 0.4 Å, whereas the RMS of deviations among the crystal structures was 0.1 Å. Thus, as can be seen in Table 1, in the crystal structures positions 67 and 323 were always hydrogen-bonded, whereas in the simulation in ~20% of the structures all atoms of Ser^{67} and Asp^{323} were located in a distance that exceeded 2.5 Å.

Computational analysis of the hydrogen-bonding pattern between position 67 and position 323 for Gβ1 mutants

Simulations of mutant Gβs such as S67K, which did not activate GIRK channels, indicated that the residues at positions 67 and 323 were always in a hydrogen-bonding distance (24). When Ser^{67} was mutated to lysine, a hydrogen-bond was formed between the side chain HZ1 or HZ2 or HZ3 of Lys^{67} and OD1 or OD2 of Asp^{323}. This hydrogen-bonding persisted 100% of the time with an average minimal distance of 1.7 Å after the system equilibrated (Fig. 2 *D*). A hydrogen-bonding distance was also seen in other mutants that did not activate GIRK channels. For example, when Asp^{323} was mutated to alanine, a hydrogen-bond between OG of Ser^{67} and HN of Ala^{323} was formed. This hydrogen-bonding persisted 95% of the time with an average length of 2.2 Å (Fig. 2 *E*). On the other hand, in the D323N mutant that activated GIRK channels, a hydrogen-bonding distance of ≤2.5 Å persisted only ~70% of the time. In this mutant, OG(Ser^{67}) interacted with either HN(Asn^{323}) or HN(Asp^{322}). Fig. 2 *F* shows the minimal distance for the D323N mutant compared to the WT minimal distance. The minimal distance for the D323N mutant was comparable to the largest values of the minimal distances for the WT.

The functional mutants S67A and S67C did not form hydrogen-bonds with Asp^{323}. The minimal distances between positions 67 and 323 for these mutants are included in Table 2. The details of hydrogen-bonding for all other mutants that formed hydrogen-bonds are shown in Tables 3 and 4. Overall, a strong correlation exists between the formation of hydrogen-bonding between positions 67 and 323 and lack of function. Although, in the absence of hydrogen-bonding other factors may play a role in determining whether the βγ-subunits of the G-protein will activate GIRK currents, G-protein mutants that formed a hydrogen-bond between position 67 and 323 (or its neighboring residues) did not activate GIRK channels (Table 4). These data suggest that the existence of hydrogen-bonding between residues 67 and 323 was detrimental to the ability of Gβ to activate GIRK channels.

Rescue of a nonfunctional mutant Gβ1(D323A) by removal of a hydrogen-bond: the double mutant Gβ1(D323A_S67A) is functional

To further test the role of hydrogen-bonding between these positions, we attempted to repair a nonactive mutant, D323A, by constructing a double mutant that would not have hydrogen-bonding between positions 67 and 323, S67A_D323A. As shown above, D323A was a nonactive mutant (Fig. 1 *D*) in which a strong H-bond existed between HN of Ala^{323} and OG of Ser^{67} (Fig. 2 *E* and Table 4). On the other hand, when Ser^{67} was mutated to alanine and the resulting mutated G-protein was functional (Fig. 1 *C*), no hydrogen-bond was formed between positions 67 and 323 of the β-subunit. Simulation of the double alanine mutant, in which both Ser^{67} and Asp^{323} were mutated to alanine, showed that this mutant lacked hydrogen-bonding between positions 67 and 323 of the β-subunit (Table 2). Following this observation, we predicted that this mutant would restore Gβ activation of GIRK channels. This prediction was confirmed experimentally by comparing the ability of this mutant to activate GIRK channels to that of the parent mutants D323A and

TABLE 2 Minimal distance simulation data between position 67 and position 323 for Gβ1γ2 mutants that lack H-bonding

Mutant	H-bonding description	Average distance (Å)	Average minimal distance (Å)
S67A	OD2(323)-HB2(67)	2.8 ± 0.3	2.6 ± 0.2
	OD1(323)-HB3(67)	2.7 ± 0.2	–
	HN(323)-HB1(67)	2.8 ± 0.2	–
S67C	HN(323)-SG(67)	2.6 ± 0.2	2.6 ± 0.2
S67A_D323A	HN(323)-HB1(67)	2.4 ± 0.2	2.4 ± 0.2
S67A_D323N	HD21(323)-HB2(67)	2.7 ± 0.3	2.6 ± 0.3
	OD1(323)-HB3(67)	3.0 ± 0.3	–

TABLE 3 Hydrogen-bonding simulation data between position 67 and position 323 (and neighboring residues) for Gβ1γ2 functional mutants

Mutant	H-bonding description	Average distance (Å)	Average angle (°)	% of H-bonding	Average minimal distance (Å)	Total % of H-bonding
WT	HN(323)-OG(67)	2.6 ± 0.3	152 ± 13	36.4%	2.1 ± 0.4	78.9%
	OD1(323)-HG1(67)	3.2 ± 1.2	95 ± 60	38.3%	–	–
	OD2(323)-HG1(67)	3.4 ± 1.0	98 ± 45	21.8%	–	–
D323N	HN(323)-OG(67)	2.4 ± 0.2	157 ± 12	68.7%	2.4 ± 0.2	69.2%
	HN(322)-OG(67)	3.0 ± 0.3	115 ± 9	1.9%	–	–

S67A. Summary data are shown in Fig. 3, where S67A and the double mutant showed similar effectiveness in stimulating GIRK currents whereas D323A did not activate the channel. An immunoblot (Fig. 3 *lower panel*) shows that expression levels for the different mutants were similar. Furthermore, a trypsin protection assay indicated proper Gβγ dimer formation (data not shown). This result implies that the presence of alanine at position 323 per se was not detrimental to activity; rather its hydrogen-bonding with Ser^{67} was the critical determinant. When the hydrogen-bonding between Ser^{67} and D323A was removed by mutating Ser^{67} to alanine, the alanine in position 323 did not have any effect on channel activation, such that both the S67A mutant and the S67A_D323A double mutant were as effective in stimulating GIRK currents. These results provide further evidence that the existence of a hydrogen-bond between positions 67 and 323 impaired Gβ activation of GIRK channels.

Other considerations in the absence of hydrogen-bonding between positions 67 and 323 of Gβ1

As shown above (see Figs. 1, *C* and *D*, and 3), we have tested the mutants for potential gross structural rearrangements due to the mutations. Specifically, we have shown proper expression of the mutants using immunoblot analysis and tested the proper interaction with Gγ, using the trypsin protection assay. Moreover, we have previously shown proper binding of several mutants of Gβ1, including S67K, to the channel. These results indicated that the mutants are expressed and properly bound to the channel and therefore do not undergo major structural rearrangements. We therefore focused on factors that most likely affect the function of the Gβγ mutants as suggested by the MD simulations. Our results are consistent with a role for hydrogen-bonding between positions 67 and 323 as a critical factor in determining Gβγ function. However, in the absence of hydrogen-bonding, other factors may also affect or even impair the ability of Gβ to enhance GIRK currents upon mutation at positions 67 and 323. Thus, while considering local structural changes, we have looked for likely candidate regions based on our findings from the MD simulations. For example, the effectiveness of the S67A mutant in enhancing GIRK channel activity is significantly reduced compared with the WT Gβ1 (e.g., Fig. 3). Examination of the effect of this mutation on nearby residues showed that compared to WT average positions, the average position of the C_α atoms of Pro^{60} and Phe^{61} in Gγ2 were displaced by 0.8 and 1.0 Å, respectively

TABLE 4 Hydrogen-bonding simulation data between position 67 and position 323 (and neighboring residues) for Gβ1γ2 nonfunctional mutants

Mutant	H-bonding description	Average distance(Å)	Average angle(°)	% of H-bonding	Average minimal distance(Å)	Total % of H-bonding
D323A	HN(323)-OG(67)	2.2 ± 0.2	157 ± 12	95.1%	2.2 ± 0.2	95.1%
D323E	OE1(323)-HG1(67)	1.8 ± 0.3	160 ± 14	97.2%	1.8 ± 0.2	99.3%
	OE2(323)-HG1(67)	2.6 ± 0.3	127 ± 10	27.9%	–	–
	HN(323)-OG(67)	2.6 ± 0.4	158 ± 11	27.6%	–	–
D323R	HH22(323)-O(67)	2.1 ± 0.3	136 ± 19	93.6%	2.0 ± 0.2	96.3%
	HH21(323)-O(67)	3.0 ± 0.3	69 ± 15	3.7%	–	–
	HN(323)-OG(67)	2.9 ± 0.2	160 ± 11	4.1%	–	–
D323L	HN(323)-OG(67)	2.3 ± 0.3	157 ± 11	84.1%	2.2 ± 0.2	95.9%
	HN(322)-OG(67)	2.6 ± 0.3	120 ± 14	32.5%	–	–
S67K	OD2(323)-HZ1(67)	2.0 ± 0.6	143 ± 45	80.7%	1.7 ± 0.1	100.0%
	OD2(323)-HZ2(67)	2.9 ± 0.6	73 ± 43	19.1%	–	–
	OD1(323)-HZ2(67)	4.2 ± 0.8	64 ± 34	8.7%	–	–
	OD1(323)-HZ1(67)	3.2 ± 0.4	121 ± 25	2.0%	–	–
	OD2(323)-HZ3(67)	3.2 ± 0.2	53 ± 9	0.3%	–	–
S67T	OD1(323)-HG1(67)	2.2 ± 0.4	145 ± 14	75.4%	1.9 ± 0.2	99.8%
	OD2(323)-HG1(67)	2.2 ± 0.4	150 ± 15	75.1%	–	–
S67Y	O(325)-HH(67)	1.8 ± 0.1	158 ± 9	100.0%	1.8 ± 0.1	100.0%

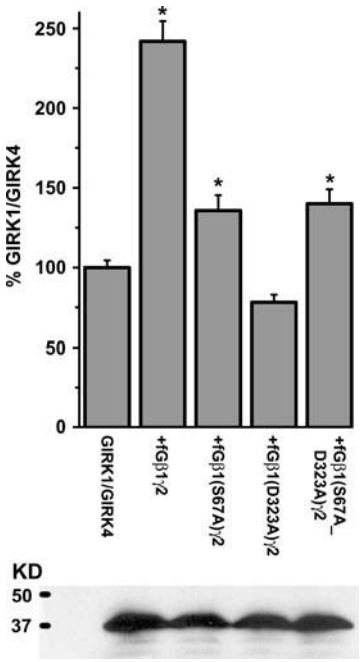

FIGURE 3 Summary data from oocytes expressing GIRK1/GIRK4 in the presence of Gγ2 and WT Gβ1 or mutants Gβ1(S67A), Gβ1(D323A), and Gβ1(S67A_D323A). Data are expressed as percentage of the control currents at −80 mV in GIRK1/GIRK4 groups. Expression of WT Gβ1 and mutants Gβ1(S67A) and Gβ1(S67A_D323A) enhanced currents significantly in comparison to GIRK1/GIRK4 alone (* $p < 0.05$, unpaired *t*-test, $n = 26$–33). Gβ1(D323A) did not significantly enhance GIRK1/GIRK4 basal current. Western blot detection of an associated Flag-tag confirmed similar expression levels for the WT Gβ1 and its mutants.

(Table 5). These two residues have been found to be critical in activation of GIRK channel by Gβ1γ2 (27). Similar displacements were obtained for the double mutant, S67A_D323A, in which the C_α atoms of Pro^{60} and Phe^{61} were displaced by 0.8 and 0.9 Å (Table 5), respectively. As a comparison, the average position of the C_α of Pro^{60} of the D323N mutant, which showed higher effectiveness in activating GIRK channel, was displaced to a lesser extent by 0.5 Å (Table 5), which is close to the fluctuation range of C_α of 0.3 Å. Thus, in the absence of hydrogen-bonding between positions 67 and 323, the data suggest that displacements of the positions of Pro^{60} and Phe^{61} affect the ability of the mutated Gβ to activate the GIRK channel. Larger displacements of Pro^{60} and Phe^{61} were observed for the double mutant S67A_D323N, which lacked hydrogen-bonding between positions 67 and 323 (Table 2). Although both the S67A and the D323N mutants were able to stimulate GIRK current, the double mutant was unable to do so (Fig. 4 *A*). An immunoblot (Fig. 4 *A lower panel*) shows that this mutant was expressed in levels similar to WT G$\beta\gamma$. Furthermore, a trypsin protection assay indicated proper G$\beta\gamma$ dimer formation (Fig. 4 *B*). The C_α atoms of Pro^{60} and Phe^{61} in the double mutant S67A_D323N were displaced by 1.1 Å and by 1.8 Å, respectively, compared to WT (Table 5). These values were significantly larger than those obtained for any other mutation. In view of the importance of Pro^{60}

TABLE 5 Simulated distance between the average position of the Cα atoms of Pro^{60} and Phe^{61} of Gγ2 in the WT Gβ1γ2 and their average position for Gβ1 mutants that lack H-bonding or form partial H-bonding between positions 67 and 323 (Å)

	S67A	S67C	D323N	S67A_D323A	S67A_D323N
Pro^{60}	0.82	0.54	0.49	0.78	1.14
Phe^{61}	1.00	0.91	0.92	0.86	1.81

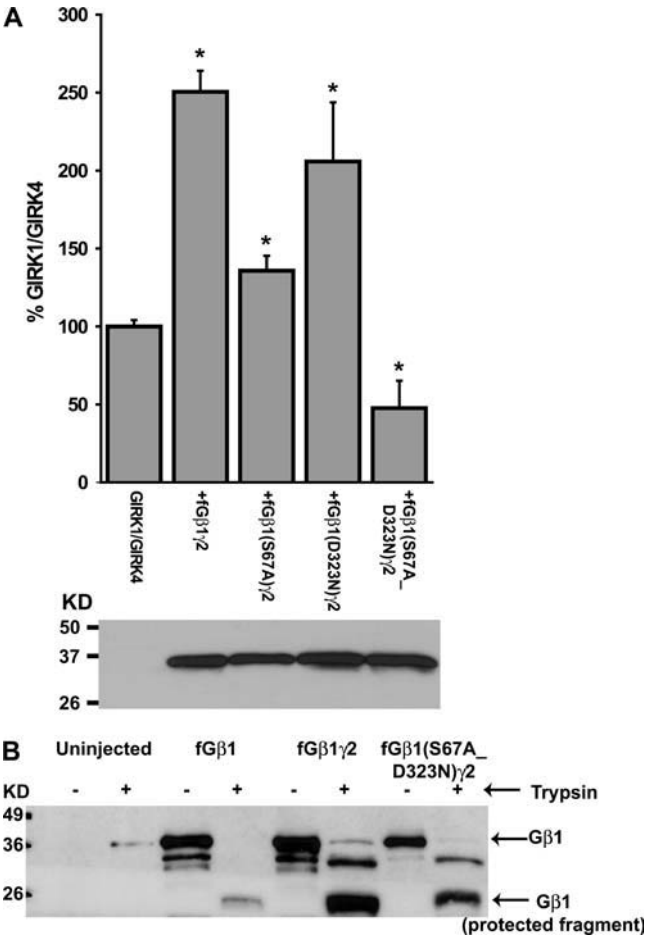

FIGURE 4 (*A*) Summary data from oocytes expressing GIRK1/GIRK4 in the presence of Gγ2 and WT Gβ1 or mutants Gβ1(S67A), Gβ1(D323N), and Gβ1(S67A_D323N). Data are expressed as percentage of the control currents at −80 mV in GIRK1/GIRK4 groups. Western blot detection of an associated Flag-tag confirmed similar expression levels for the WT Gβ1 and its mutants. (*B*) Gβ1(S67A_D323N) interacts properly with Gγ2. Partial trypsin protection assays of uninjected oocytes or oocytes injected with cRNA for Flagβ1 alone, Flagβ1γ2, and Flagβ1(S67A_D323N)γ2. Uninjected oocytes showed no major proteins bands. Untreated samples show a ~37-KDa band that corresponds to full length Gβ1. The 37 KDa band from fGβ1 alone was almost completely digested by trypsin. The 26-kDa C-terminal Gβ1 fragment that is protected by Gγ2 is seen in lanes with fGβ1γ2 and fGβ1(S67A_D323N)γ2, indicating proper interaction between the two proteins. The weak protected band in the lane with fGβ1 alone could result from protection by endogenous Gγ.

and Phe[61] in Gγ2 in activation of GIRK channel by Gβ1γ2 (27), the large displacements of these two residues in the double mutant S67A_D323N may account for its inability to stimulate GIRK currents.

DISCUSSION

The crystal structures available for Gβγ show that in general they maintain a rigid structure in different states as well as in complex with different proteins. MD simulations suggest that fluctuations in interatomic distances within important domains in Gβ1 are critical in its ability to activate GIRK channels. Specifically, Ser[67] and Asp[323] of Gβ1 are part of a functionally important region that includes, for example, Pro[60] and Phe[61] of Gγ2. Our findings suggest that interactions between positions 67 and 323 are critical in GIRK channel activation by Gβ1. Distinct sites on Gβγ regulate specific functions on the channels (21). The region studied in this work is clearly a critical functional determinant of channel activation even though the relationship with other regions and the specific roles each region plays remain to be further defined.

We previously emphasized the importance of Ser[67] in basal GIRK currents. Since Ser[67] is independent of interactions with the Gα-subunit, we tested the ability of the mutant Gβ1(S67K) to inhibit basal currents (presumably by competing away native Gβγ—a dominant negative effect) (4,30) using a GIRK4*(L339E) mutant that showed Gβγ-dependent basal currents but failed to show agonist-induced currents. GIRK4* is the homotetrameric active GIRK4(S143T) channel (31). Indeed, Gβ1(S67K) inhibited GIRK4*(L339E) currents whereas another mutant, Gβ1(S98T), that did interact with Gα did not reduce GIRK currents (4). Furthermore, although mutations such as Gβ1(S67K) did not activate GIRK channels in whole-cell or in inside-out patches, they did bind the N- and C-termini of the channel (21). These results suggested that the lack of activation by Gβ1(S67K) is not due to binding defects. In addition, although Gβ1(S67K) in itself could not activate K^+ currents in inside-out patches, it could fully support the increased sodium activation of the channel similar to the WT Gβ1 (21). This implied that the Gβ1(S67K) mutant induces a specific functional defect that is related to channel activation rather than a defect in binding to the channel.

In this study we have studied further the importance of this critical Gβ1 residue Ser[67] in channel activation as well as of Asp[323], which is located in its vicinity. We focused on testing for effects of a number of mutants at these positions on basal currents. Some mutants had either an inhibitory or no effect (S67T, S67Y, D323A, D323E, D323L, and D323R). Other mutations of S67 showed a significant stimulation of basal currents (S67A, S67C, and D323N). All Ser[67] and Asp[323] mutants showed high expression levels and were processed properly as assayed by interactions with Gγ. Thus, these observations lend further support to the notion that Ser[67] is a critical functional determinant of Gβγ activation of GIRK currents, and as shown in this work its interaction with Asp[323] is critical to its effects.

Simulation of the WT Gβ1 suggests a dynamic protein that fluctuates between different hydrogen-bonded conformations. Hydrogen-bonds are formed between HN(Asp[323]) and OG(Ser[67]) as well as between OD1,2(Asp[323]) and HG1 (Ser[67]) (See Fig. 2 *B*). There are, however, continuous periods in which neither of these hydrogen-bonds are present (Fig. 2 *C*). Our results identified a set of mutants that abolished Gβγ activity. The simulations show that these mutants that include, for example, S67K and D323A (see Fig. 6 *E*), form stable hydrogen-bonds between positions 67 and 323 with an average minimal distance ranging from 1.7 Å (S67K) to 2.2 Å (e.g., D323A). This suggests that the WT Gβγ can activate GIRK channels only during periods in which there is no hydrogen-bonding between positions 67 and 323 (Figs. 2 *C* and 6 *A*). The role of hydrogen-bonding between positions 67 and 323 was further supported by the rescue of D323A function by the double mutant S67A_D323A. Mutation of Ser[67] to alanine in addition to the D323A mutation removed the hydrogen-bonding detected between positions 67 and 323 in simulations from the inactive D323A mutant (Figs. 3 and 6, *B* and *E*). Mutants that displayed partial hydrogen-bonding (e.g., D323N) or no hydrogen-bonding (e.g., S67A) between positions 67 and 323 enabled activation of GIRK channel by Gβγ (Fig. 6, *A* and *B*).

Another interesting finding of these studies was that the double mutant S67A_D323N that is based on two functional single mutants was not functional (Fig. 4). Hydrogen-bonds were not detected between Ala[67] and Asn[323] in simulations of this mutant. However, closer examination showed large displacements in Gγ2 residues Pro[60] and Phe[61] that are critical in activating GIRK channels (Table 5 and Fig. 6 *D*). While we have shown that presence of a hydrogen-bond between residues 67 and 323 is detrimental to the ability of Gβγ to activate GIRK channels, other factors could also affect this activity. These can be changes on critical neighboring residues as observed for the S67A_D323N double mutant. Other structural changes caused by mutations could affect the activity in unpredictable ways, which may explain the reduced activity of mutants S67A and S67C compared to the WT Gβγ although both mutants lack hydrogen-bonds at this site.

Furthermore, in the presence of hydrogen-bonding, mutations at positions 67 and 323 in Gβ1 may also lead to additional harmful consequences. In particular these mutations may also affect positions 60 and 61 in Gγ2. Most of the mutants that we have tested, however, do not show large displacements of these positions, as seen in Table 6. For example, the D323L mutant shows displacements for both Pro[60] and Phe[61] that are comparable to the displacements observed for the functional D323N mutant (see Tables 5 and 6) and therefore cannot account for the lack of activity of this mutant (Fig. 6 *C*). Examination of the effect of the mutations

TABLE 6 Simulated distance between the average position of the Cα atoms of Pro^{60} and Phe^{61} of Gγ2 in the WT Gβ1γ2 and their average position for Gβ1 mutants that form strong H-bonding between positions 67 and 323 (Å)

	S67K	S67T	S67Y	D323A	D323E	D323L	D323R
Pro^{60}	1.09	0.93	0.86	0.98	0.75	0.46	0.68
Phe^{61}	0.92	2.21	0.56	1.40	0.78	0.49	0.87

on other residues, which have been found to be important in activation of GIRK channel by Gβ1γ2, such as Thr^{86}, Thr^{87}, and Asn^{88} in Gβ1 (2) and Pro^{49} in Gγ2 (27) did not show significant displacements of these residues for the D323L mutant. The most significant difference between the WT and the D323L mutant is the formation of a stable hydrogen-bond between positions 67 and 323, which as our data suggest, impairs the ability of G$\beta\gamma$ to activate GIRK channels.

Fig. 5 displays the maximal of the displacements of the average positions of the α-carbons of Pro^{60} and Phe^{61} of Gγ2 relative to the WT Gβ1γ2 as a function of the minimum average distance between positions 67 and 323 for each of the mutants that we tested. As can be seen in the figure, all mutants that enhance GIRK currents are clustered in the quarter in which the minimum distance between positions 67 and 323 is 2.4 Å or larger, and the larger of the displacements of the α-carbons of Pro^{60} and Phe^{61} of Gγ2 does not exceed 1 Å. Thus, the clustering suggests approximate limiting values of the two factors discussed above that constitute a prerequisite for the ability of Gβ1γ2 to activate GIRK channels.

Fig. 6 summarizes schematically the different possibilities suggested regarding the structural implications of mutations at positions 67 and 323 of Gβ1 and their effect on the ability of G$\beta\gamma$ to activate GIRK channels. Fig. 6, *A* and *B*, represents Gβ1 and its mutants that activate GIRK channels.

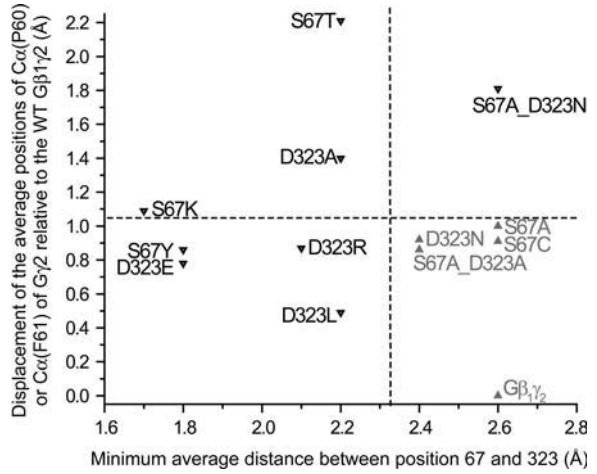

FIGURE 5 The maximal of the displacements of the average positions of the α-carbons of Pro^{60} and Phe^{61} of Gγ2 relative to the WT Gγ2 (Tables 5 and 6) as a function of the minimum average distance between positions 67 and 323 of their mutants (Tables 2–4). The corresponding summary data from oocytes expressing GIRK1/GIRK4 in the presence of Gγ2 and WT Gβ1 or mutants are included in Figs. 1, 3, and 4. The gray-filled triangles indicate mutants that enhanced GIRK currents, and the black inverted triangles indicate mutants that did not enhance GIRK currents.

These mutants have an insignificant effect on the interactions between positions 67 and 323 of Gβ1 (position I) and a limited effect on other critical residues, such as Pro^{60} and Phe^{61} of Gγ2 (position II). Fig. 6, *C–E*, represents mutations that impair the ability of G$\beta\gamma$ to activate GIRK channels. Our results suggest that either hydrogen-bonding between positions 67 and 323 (Fig. 6 *C*) or the effect on other critical residues (Fig. 6 *D*) or both could impair the ability of G$\beta\gamma$ to activate GIRK channels (Fig. 6 *E*). This is depicted as an impaired fit at positions I and/or II.

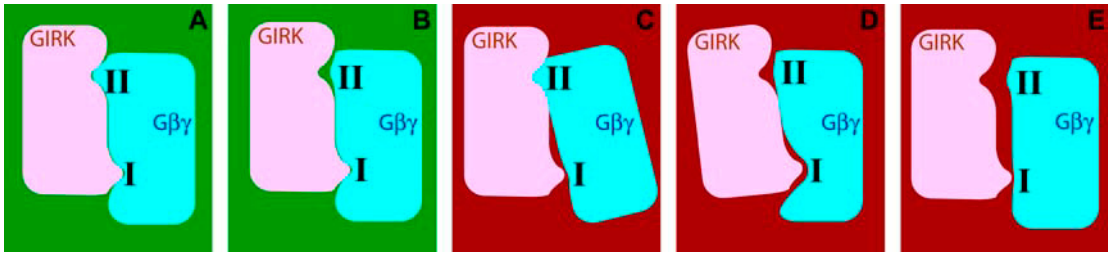

FIGURE 6 Schematic model of the different possibilities regarding the structural changes in G$\beta\gamma$ after mutations at positions 67 and 323 of Gβ1. The pink-colored shape represents GIRK, and the cyan-colored shape represents G$\beta\gamma$. Position I represents the interaction between positions 67 and 323. Position II represents the effect of mutations at these two positions on other critical residues. The green background indicates active mutants, and the red indicates inactive ones. (*A*) This figure represents the functional WT Gβ1 as well as mutants such as D323N that enhance GIRK channel activity. In these cases, the functional G$\beta\gamma$ fits precisely to GIRK channels. (*B*) Mutations that have insignificant effect on the interactions between positions 67 and 323 of Gβ1 and a limited effect on other crucial residues enhance GIRK currents to a reduced extent compared to WT. This is represented in the figure as an imprecise fit between G$\beta\gamma$ and GIRK at position II. Mutations in this group include, for example, S67A, and S67A_D323A. (*C*) Mutations that lead to stable hydrogen-bonding impair the ability of G$\beta\gamma$ to activate GIRK channels, as depicted in the figure as an impaired fit at position I; examples include D323E, D323L, and D323R. (*D*) Mutations such as S67A_D323N that result in an increase in the minimal average distance between positions 67 and 323 of Gβ1 and affect other crucial positions such as positions 60 and 61 of Gγ2, also abolish G$\beta\gamma$ activity. (*E*) Mutations that lead to stable hydrogen-bonding between positions 67 and 323 of Gβ1 but also affect other crucial positions are depicted in this figure by the impaired fit at both positions I and II. These mutated β1-subunits do not enhance GIRK currents. In this group included are, for example, D323A and S67T.

Thus, the relationship between GIRK channel activation by Gβ1 and hydrogen-bonding between positions 67 and 323 suggests that the dynamic nature of the hydrogen-bonding pattern in the WT serves an important functional role that regulates GIRK channel activation by Gβγ. It is likely that the local flexibility portrayed by the WT Gβ1 enables it to acquire the appropriate conformation for activating the channel. This conformation could become the dominant conformation of Gβ1 upon its binding to GIRK. Our results suggest that the dynamic regulation of the interactions between Gβγ and effectors provides for a complex regulatory process in cellular functions.

This work was supported by an NRSA National Institutes of Health Award and a Scientist Development Grant from the American Heart Association (T.M.) and by a National Institutes of Health grant HL54185, (D.E.L.). D.E.L. is an Established Investigator of the American Heart Association.

REFERENCES

1. Bunemann, M., M. Frank, and M. J. Lohse. 2003. Gi protein activation in intact cells involves subunit rearrangement rather than dissociation. *Proc. Natl. Acad. Sci. USA.* 100:16077–16082.
2. Ford, C. E., N. P. Skiba, H. Bae, Y. Daaka, E. Reuveny, L. R. Shekter, R. Rosal, G. Weng, C. S. Yang, R. Iyengar, R. J. Miller, L. Y. Jan, R. J. Lefkowitz, and H. E. Hamm. 1998. Molecular basis for interactions of G protein betagamma subunits with effectors. *Science.* 280:1271–1274.
3. Buck, E., J. Li, Y. Chen, G. Weng, S. Scarlata, and R. Iyengar. 1999. Resolution of a signal transfer region from a general binding domain in Gbeta for stimulation of phospholipase C-beta2. *Science.* 283:1332–1335.
4. Mirshahi, T., L. Robillard, H. Zhang, T. E. Hebert, and D. E. Logothetis. 2002. Gbeta residues that do not interact with Galpha underlie agonist-independent activity of K^+ channels. *J. Biol. Chem.* 277:7348–7355.
5. Medina, R., G. Grishina, E. G. Meloni, T. R. Muth, and C. H. Berlot. 1996. Localization of the effector-specifying regions of Gi2alpha and Gqalpha. *J. Biol. Chem.* 271:24720–24727.
6. Scott, J. K., S.-F. Huang, B. P. Gangadhar, G. M. Samoriski, P. Clapp, R. A. Gross, R. Taussig, and A. V. Smrcka. 2001. Evidence that a protein-protein interaction 'hot spot' on heterotrimeric G protein betagamma subunits is used for recognition of a subclass of effectors. *EMBO J.* 20:767–776.
7. Sondek, J., A. Bohm, D. G. Lambright, H. E. Hamm, and P. B. Sigler. 1996. Crystal structure of a G-protein beta gamma dimer at 2.1 Å resolution. *Nature.* 379:369–374.
8. Wall, M. A., D. E. Coleman, E. Lee, J. A. Iniguez-Lluhi, B. A. Posner, A. G. Gilman, and S. R. Sprang. 1995. The structure of the G protein heterotrimer Gi alpha 1 beta 1 gamma 2. *Cell.* 83:1047–1058.
9. Gaudet, R., A. Bohm, and P. B. Sigler. 1996. Crystal structure at 2.4 angstroms resolution of the complex of transducin betagamma and its regulator, phosducin. *Cell.* 87:577–588.
10. Lodowski, D. T., J. A. Pitcher, W. D. Capel, R. J. Lefkowitz, and J. J. G. Tesmer. 2003. Keeping G proteins at bay: a complex between G protein-coupled receptor kinase 2 and Gbetagamma. *Science.* 300: 1256–1262.
11. Clapham, D. E., and E. J. Neer. 1997. G protein beta gamma subunits. *Annu. Rev. Pharmacol. Toxicol.* 37:167–203.
12. Logothetis, D. E., Y. Kurachi, J. Galper, E. J. Neer, and D. E. Clapham. 1987. The beta gamma subunits of GTP-binding proteins activate the muscarinic K^+ channel in heart. *Nature.* 325:321–326.
13. Reuveny, E., P. A. Slesinger, J. Inglese, J. M. Morales, J. A. Iniguez-Lluhi, R. J. Lefkowitz, H. R. Bourne, Y. N. Jan, and L. Y. Jan. 1994. Activation of the cloned muscarinic potassium channel by G protein beta gamma subunits. *Nature.* 370:143–146.
14. Sui, J. L., K. W. Chan, M. N. Langan, M. Vivaudou, and D. E. Logothetis. 1999. G protein gated potassium channels. *Adv. Second Messenger Phosphoprotein Res.* 33:179–201.
15. Kubo, Y., E. Reuveny, P. A. Slesinger, Y. N. Jan, and L. Y. Jan. 1993. Primary structure and functional expression of a rat G-protein-coupled muscarinic potassium channel. *Nature.* 364:802–806.
16. Lesage, F., F. Duprat, M. Fink, E. Guillemare, T. Coppola, M. Lazdunski, and J. P. Hugnot. 1994. Cloning provides evidence for a family of inward rectifier and G-protein coupled K^+ channels in the brain. *FEBS Lett.* 353:37–42.
17. Dascal, N. 1997. Signaling via the G protein-activated K^+ channels. *Cell. Signal.* 9:551–573.
18. Yamada, M., A. Inanobe, and Y. G. Kurachi. 1998. Protein regulation of potassium ion channels. *Pharmacol. Rev.* 50:723–757.
19. Krapivinsky, G., E. A. Gordon, K. Wickman, B. Velimirovic, L. Krapivinsky, and D. E. Clapham. 1995. The G-protein-gated atrial K^+ channel IKACh is a heteromultimer of two inwardly rectifying K^+-channel proteins. *Nature.* 374:135–141.
20. Albsoul-Younes, A. M., P. M. Sternweis, P. Zhao, H. Nakata, S. Nakajima, Y. Nakajima, and T. Kozasa. 2001. Interaction sites of the G protein beta subunit with brain G protein-coupled inward rectifier K^+ channel. *J. Biol. Chem.* 276:12712–12717.
21. Mirshahi, T., V. Mittal, H. Zhang, M. E. Linder, and D. E. Logothetis. 2002. Distinct sites on G protein beta gamma subunits regulate different effector functions. *J. Biol. Chem.* 277:36345–36350.
22. Beglov, D., and B. Roux. 1995. Dominant solvation effects from primary shell of hydration: approximation for molecular dynamics simulations. *Biopolymers.* 35:171–178.
23. Brooks, B. R., R. Bruccoleri, B. Olafson, D. States, S. Swaminathan, and M. Karplus. 1983. CHARMM: a program for macromolecular energy, minimization, and dynamics calculations. *J. Comput. Chem.* 4:187–217.
24. McDonald, I. K., and J. M. Thornton. 1994. Satisfying hydrogen-bonding potential in proteins. *J. Mol. Biol.* 238:777–793.
25. Chan, K. W., J. L. Sui, M. Vivaudou, and D. E. Logothetis. 1996. Control of channel activity through a unique amino acid residue of a G protein-gated inwardly rectifying K^+ channel subunit. *Proc. Natl. Acad. Sci. USA.* 93:14193–14198.
26. Sui, J. L., K. W. Chan, and D. E. Logothetis. 1996. Na^+ activation of the muscarinic K+ channel by a G-protein-independent mechanism. *J. Gen. Physiol.* 108:381–391.
27. Peng, L., T. Mirshahi, H. Zhang, J. P. Hirsch, and D. E. Logothetis. 2003. Critical determinants of the G protein gamma subunits in the Gbetagamma stimulation of G protein-activated inwardly rectifying potassium (GIRK) channel activity. *J. Biol. Chem.* 278:50203–50211.
28. Wall, M. A., B. A. Posner, and S. R. Sprang. 1998. Structural basis of activity and subunit recognition in G protein heterotrimers. *Structure.* 6:1169–1183.
29. Rahmatullah, M., and J. D. Robishaw. 1994. Direct interaction of the alpha and gamma subunits of the G proteins. Purification and analysis by limited proteolysis. *J. Biol. Chem.* 269:3574–3580.
30. Lei, Q., M. B. Jones, E. M. Talley, A. D. Schrier, W. E. McIntire, J. C. Garrison, and D. A. Bayliss. 2000. Activation and inhibition of G protein-coupled inwardly rectifying potassium (Kir3) channels by G protein beta gamma subunits. *Proc. Natl. Acad. Sci. USA.* 97:9771–9776.
31. Vivaudou, M., K. W. Chan, J. L. Sui, L. Y. Jan, E. Reuveny, and D. E. Logothetis. 1997. Probing the G-protein regulation of GIRK1 and GIRK4, the two subunits of the KACh channel, using functional homomeric mutants. *J. Biol. Chem.* 272:31553–31560.